Toward automated detection and segmentation of aortic calcifications from radiographs

François Lauze[a] and Marleen de Bruijne[b]

[a]Nordic Bioscience Imaging, Herlev Hovegade 207, 2370 Herlev, Denmark
[b]DIKU, University of Copenhagen, Universitetsparken 1, Copenhagen, Denmark

ABSTRACT

This paper aims at automatically measuring the extent of calcified plaques in the lumbar aorta from standard radiographs. Calcifications in the abdominal aorta are an important predictor for future cardiovascular morbidity and mortality. Accurate and reproducible measurement of the amount of calcified deposit in the aorta is therefore of great value in disease diagnosis and prognosis, treatment planning, and the study of drug effects. We propose a two-step approach in which first the calcifications are detected by an iterative statistical pixel classification scheme combined with aorta shape model optimization. Subsequently, the detected calcified pixels are used as the initialization for an inpainting based segmentation. We present results on synthetic images from the inpainting based segmentation as well as results on several X-ray images based on the two-steps approach.

Keywords: Atherosclerosis, X-Ray imaging, Tissue Classification, Particle Filtering, Inpainting, Active Contours

1. INTRODUCTION

Atherosclerosis is a disease that affects a large portion of the population[1–3] and causes various cardiovascular events and subsequent cardiovascular disease mortality.[3] Already in the 1950's focus was brought to atherosclerosis in an autopsy study by Eggen *et al.*,[1] which reported highly significant correlations between the degree of calcification in the lumbar aorta and the presence of plaque in the coronary arteries.[4–7] This work is a step toward the development of a mass-screening tool for the automated detection and segmentation of X-Ray images of calcific deposits in the lumbar aortic region. Although several automated and semi automated methods have been previously proposed for use in CT images, see for instance Higgins *et al.*,[8] to our knowledge no method by other authors currently exists for automated segmentation of calcified plaques from X-ray images. Segmentation of calcifications in X-rays is more complicated than in CT images as a large number of structures in the image, e.g. bone and image artifacts, have a similar appearance as calcification, whereas soft tissue such as the aorta itself is invisible.

Because of the planar X-Ray imaging, calcific deposits are predominantly situated along the aortic walls, a fact used in the somewhat crude but de facto golden standard Framingham score,[9] a discrete score in a range from 0 to 24, normally computed by radiologists through manual inspection of the images. These walls, i.e. the boundaries of the aorta, are normally not visible with this imaging modality, as this is the case for most of the soft tissues. Their locations can nevertheless be inferred from the location of the spine in the form of a probability distribution conditioned by the location of the spine. The presence of a calcific deposit is also a strong clue for the location of the aortic walls. This and a pixel classification scheme based on a prior training on calcification tightly coupled to it, provide the detection step of our method. This step has been investigated and described on its own by the second author in[10, 11]

For the segmentation part we have developed a region based active contour approach, that can be interpreted as the segmentation of a background substraction image, where however the background is unknown and must be estimated based on the current observation and some prior statistical knowledge on admissible background

Further author information: (Send correspondence to François Lauze)
François Lauze: E-mail: francois@diku.dk
Marleen de Bruijne: E-mail: marleen@diku.dk

Medical Imaging 2007: Image Processing, edited by Josien P. W. Pluim, Joseph M. Reinhardt,
Proc. of SPIE Vol. 6512, 651239, (2007) · 1605-7422/07/$18 · doi: 10.1117/12.709328

images. A standard region based approach à la Chan and Vese[12] is generally bound to fail du to the complexity of the background. Other methods incorporating for instance higher order statistical moments will present the same difficulties. Two important phenomena are encountered in this situation: background non stationarity and transparency. Instead of trying to provide higher order models for the statistical content of these images, we try in fact to cancel it out with the help of background substraction. This step has been described and studied on its own by the first author in.[13] This step has been motivated by a series of work on inpainting of X-rays performed in our team (see L. Conrad-Hansen *et al.*[14,15]).

The paper is organized as follows. In the next section, we present the combined pixel classification – particle filter approach we have used for the detection of calcifications. Then in Section 3.1 we review briefly active contours and we introduce the inpainting driven segmentation algorithm used as second step in our method. We also discuss how specific knowledge on the aorta location can be added at that step. In Section 4 we present a series of numerical experiences on aortic X-rays, demonstrating several aspects of our work: the detection step, the active contour mechanism, experiments on the two steps detection – segmentation, and examples of segmentation with incorporation of aortic wall data. We also compare segmentation results with the ground truth obtained by radiologists via average area overlap. We summarize and conclude our work in Section 5.

2. CALCIFICATION DETECTION

Areas of calcified plaque in the images can be detected by classifying all pixels individually in calcium or background, using pattern classification techniques[16] and image appearance features such as image intensity. As many image structures in X-rays appear locally similar to aortic calcifications this often results in many false positive detections.

Results of standard pixel classification can be improved by incorporating a spatially varying prior that gives the probability of a pixel containing calcium, dependent on the position in the image. The spatially varying prior is derived from a statistical model of aorta shape variation together with a model of how the calcium is distributed within the aorta. The individual steps and joint optimization of classification and shape are described below; for a more detailed explanation on shape guided classification see.[11]

2.1. Pixel classification

An initial classification, based on appearance information alone, can be obtained using a pixel classifier trained to distinguish between calcium and background pixels on the basis of local image descriptors. In this paper, the pixels are described by the outputs of a set of Gaussian derivative filters at multiple scales, and a k nearest neighbor (k-NN) classifier is used for probability estimation. The probability that a pixel with feature vector $\mathbf{x}$ belongs to class ω_c is then given by

$$P(\omega_c|\mathbf{x}) = \frac{k_{\omega_c}}{k}, \tag{1}$$

where k_{ω_c} among the k nearest neighbors belong to class ω_c.

2.2. Shape guided classification

Knowledge about the aorta shape and location would be needed for a more accurate discrimination between true and false positives. However, the (uncalcified) aorta itself is not visible in the image. We therefore assume that the corner points of the vertebræ, which are more easily discernible in the image, have been indicated — either manually or automatically[17,18] — and use as an aorta shape prior a Gaussian conditional shape model that describes the expected pose and shape variation of the aorta with respect to the known spine landmarks. The distribution of calcium with respect to the aorta is estimated from a training set of manually annotated example images. Typically, calcium is found of course only inside the aorta and, due to the projection imaging, mostly along the aortic walls.

The aim of shape guided classification is to find an image labeling C which is consistent with both the image I and the prior aorta shape model $P(S)$. To this end, the joint posterior probability distribution $P(C, \mathcal{S}|I)$ for the labeling C and a set of shape samples $\mathcal{S}$ is sought using an iterative procedure:

Start with an initial labeling estimate C^0 (the original pixel classification) and shape set $\mathcal{S}^0 = \{S_1, S_2, \ldots, S_N\}$ sampled randomly from the prior shape model $P(S)$

Iterate:

1. Sample $\mathcal{S}^t$ from $P(S|C^{t-1}, I, \mathcal{S}^{t-1})$
2. Set estimate $C^t = \text{argmax}_C P(C|I, \mathcal{S}^t)$

In the first step, a new shape set $\mathcal{S}^t$ is sampled from the current shape set $\mathcal{S}^{t-1}$ using likelihood weighting based on the current classification estimate. The shape particle distribution is thus evolved under the influence of the current classification, one step towards the (global) optimization of $P(S|C^{t-1}, I)$. In the second step, the classification estimate is updated with the shape prior from the new shape set. In this way, the statistical classification is moderated with prior information from a shape model, whereas the variance in this shape prior decreases as image evidence for preferring some shapes above others is accumulated. Since a large number of shape hypotheses is used this method does not easily get trapped in local maxima.

To simplify optimization, we assume that the two individual class probabilities, based on appearance and on position with respect to aorta shape, are independent. The classification estimate in step 2 of each iteration is then given by the multiplication of the initial classification estimate with the current shape prior:

$$C^t(j, c) = P(\omega_{cj}|\mathbf{x}_j, \mathcal{S}^t) = P(\omega_c|\mathbf{x}_j)P(\omega_{cj}|\mathcal{S}^t) = C^0 P(\omega_{cj}|\mathcal{S}^t), \tag{2}$$

where $_j$ is a pixel index and $P(\omega_{cj}|\mathcal{S})$, the class probabilities due to a shape collection, is simply the average of all individual probability maps:

$$P(\omega_{cj}|\mathcal{S}) = \sum_i P(\omega_{cj}|S_i)P(S_i). \tag{3}$$

The calcification detection step is illustrated in Figure 1, corresponding parameters are briefly discussed in the Results and Experiments Section (Section 4).

3. SEGMENTATION

3.1. A brief review of Active Contours

Active contours were introduced by Kass, Witkin and Terzopoulos[19] and are now a standard segmentation tool in computer vision and medical imaging, for they allow to overcome the locality problem of edge detectors. They are curves with built in regularity properties and preferences for edges in an image. They often suffer among other of initialization problems and necessitate reparameterization, but are very simple to implement in the other hand. In order to overcome initialization problems several solutions were proposed, including balloon forces,[20] gradient vector flows.[21] Geodesic active contours, proposed independently by Caselles *et al.*[22] and Kichenassamy *et al.*[23] introduced a parameterization independent formulation. All these models deal only with contours, not with the regions they separate. Based on a simplification of the Mumford-Shah segmentation functional,[24] Chan and Vese proposed a region based algorithm in,[12] that leads to a contour evolution coupled with the estimation of the mean values in the regions delimited by this contour. More complex statistical descriptors have been proposed instead of the mean, as histogram matching in.[25] Paragios and Deriche haved proposed the Geodesic Active Regions where both contour based and region based terms are used (see for instance[26]). Many declinations on these ideas have been proposed in order to tackle the variety of situation encountered in Computer Vision and Medical Imaging. We note nevertheless that in region based active contours, the different regions one want to recover form, together with their boundaries, a partition of the image domain, and that the respective contents of these regions are usually assumed to be independent of each others. When the object/signal to be detected does not occlude the background but is added to it via some form of intensity superposition, linear or not,[27] this independence is generally no longer true (except in some Gaussian distribution cases). Another limitation of the above mentioned region approaches is that they use some form of stationarity for the distributions in each regions.

3.2. Inpainting based Active Contours

In order to overcome these limitations we have developed an approach based on the following assumptions and rationale. Assume we are given a background image I_b, defined on the image domain D, it would be an ideal noise-free X-ray of an healthy aorta, and that an object located at $\tilde{\Omega} \subset D$, is added by superposition, a calcific deposit in this work, and with the unavoidable noise, that we assume white, providing the observed image I. One can form the pixelwise difference image $J = I - I_b$, or a more complex discrepancy image $J = L(I_b, I)$ for a non linear superposition, we will however concentrate in this work in a simple discrepancy function L, the pixel difference and the absolute value pixel difference. A grouping/segmentation algorithm applied on this discrepancy image should provide the location and thus segmentation of the object of interest. Such a segmentation algorithm, that we mentioned above is the Chan and Vese one, that attempts at discriminating two regions as the ones whose intensity means are as far apart as possible, with some added regularity such as limited region/boundary size. In our case, the region of the image J not containing the object is expected to have a zero mean, and the Chan and Vese algorithm simplifies in computing the region Ω such that the average (in absolute value)

$$\mathcal{G}(\Omega; I_b, I) = \frac{1}{|\Omega|} \left| \int_\Omega J \, dx \right|$$

is as large as possible ($|\Omega|$ is the area of the region Ω), with some regularity condition on Ω. We will consider a slightly more general form

$$\mathcal{G}(\Omega; I_b, I) = \frac{1}{|\Omega|^p} \left| \int_\Omega L(I, I_b) \, dx \right|, \quad p \in [0, 1]. \tag{4}$$

Let us now assume that if the location $\tilde{\Omega}$ of the calcific deposit is known in the image I, we have an *inpainting* or *background recovery* operator $\mathcal{I}(I, \tilde{\Omega})$ which provides a reliable estimate $\bar{I}_b$ of the background image I_b. Then we expect $\tilde{\Omega}$ to maximize the above segmentation criterion, with $\mathcal{I}(I, \tilde{\Omega})$ substituted to I_b. We may therefore seek $\tilde{\Omega}$ as the subdomain of the image domain D maximizing the constrained criterion, which can be interpreted as background recovery quality measure

$$\begin{cases} \mathcal{H}(\Omega) = & \frac{1}{|\Omega|^p} \left| \int_\Omega L(I, I_b) \, dx \right| \\ I_b = & \mathcal{I}(I, \Omega). \end{cases} \tag{5}$$

3.3. About the optimization

This problem belongs to the class of optimal shape control problems. A general form for this type of problem is the following: given a *control space* C and a *state space* S, one want to optimize a given criterion $F : \mathcal{C} \times \mathcal{S} \to \mathbb{R}$, i.e. find the (a) optimal pair $(c, s) \in \mathcal{S} \times \mathcal{C}$ for F, under the *state equation* constraint $S(c, s) = 0$. In our problem, the control space is a space of subdomains Ω of D, with a certain regularity, the state space is a space of functions $u : D \to \mathbb{R}$ with some regularity conditions and the state equation for the problem is $S(\Omega, u) = u - \mathcal{I}(\Omega, I) = 0$.

In this work, we have focused on a simple variational formulation for the background recovery operator definition, the recovered background – which is the state associated to the control domain Ω, is the minimizer of the following energy

$$\mathcal{F}(J; I, \Omega) = \frac{\lambda}{2} \int_{D \setminus \Omega} (J - I)^2 + \int_D \frac{1}{r} \langle |\nabla v| \rangle_\varepsilon^r \, dx \tag{6}$$

where $\langle t \rangle_\varepsilon = \sqrt{t^2 + \varepsilon^2}$ is sometimes called the "Japanese Bracket", ε is a small positive real number and $r \in [1, 2]$. When $r = 1$, this corresponds to a regularized version of the Total Variation Inpainting and Denoising formulation of Chan and Shen.[28] A minimizer of this energy belongs to the Sobolev space $W^{1,r}(D)$ if $r > 1$ and the space $BV(D)$ of functions of bounded variations in D if $r = 1$, and is a denoised version of I outside the domain Ω.

Calculus of variations allows us to compute thís minimizer as the solution of a partial differential equation (PDE) depending on the region Ω and the observed image I. This PDE is the state equation of our problem. It will be stated below in formula (8).

Using geometrical techniques thoroughly described by Delfour and Zolésio[29], this leads to a coupled system of partial differential equations: a contour evolution equation, an inpainting equation, and a linear elliptic equation which is known as the adjoint state equation of the problem. If we let $\Gamma(t)$ be the contour of the region $\Omega(t)$ which ought to maximize (5) at steady state ($t \to \infty$), $I_b(t)$ be the corresponding state, i.e. the inpainting of I inside $\Omega(t)$, together with the adjoint state variable $\xi(t)$, then the triple $(\Gamma(t), I_b(t), \xi(t))$ solves

$$\text{Contour:} \qquad \frac{\partial \Gamma}{\partial t} = S\left(p\frac{\mathcal{H}(\Omega)}{|\Omega|} - \frac{L(I_b, I)_{|\Gamma}}{|\Omega|^p} - \lambda(I_b - I)\xi_{|\Gamma}\right)\vec{n} \tag{7}$$

$$\text{Inpainting:} \qquad \lambda\chi_{D\setminus\Omega}(I_b - I) - \operatorname{div}\left(\langle|\nabla I_b|\rangle_\varepsilon^{r-2}\nabla I_b\right) = 0 \tag{8}$$

$$\text{Adjoint state:} \qquad \lambda\chi_{D\setminus\Omega}\xi - \operatorname{div}\left(A(\nabla I_b)\xi\right) = \chi_\Omega \frac{L_x(I_b, I)}{|\Omega|^p} \tag{9}$$

where S is the sign of $\int_\Omega L(I_b, I)\,dx$, $\vec{n}$ is the inward normal to Γ, $A(\nabla I_b)$ is the Hessian of the function $(\alpha, \beta) \mapsto \frac{1}{r}\sqrt{\alpha^2 + \beta^2 + \varepsilon^2}^r$ computed at $(\alpha, \beta)^T = \nabla I_b$, and for a subset E of D, χ_E denotes its characteristic function, $\chi_E(x) = 1$ if $x \in E$ and $\chi_E(x) = 0$ otherwise. More details, in a slightly different form can be found in a previous work[13] of the first author. The resulting evolution is implemented in the framework of level sets following the work of Sethian:[30] $\Gamma(t)$ is represented by the zero-th level set of a function $\phi(-, t)$, while $\Omega(t)$ corresponds to $\{x, \phi(x, t) < 0\}$ and $D\setminus\Omega(t)$ to $\{x, \phi(x, t) > 0\}$ and $\phi(-, t)$ i chosen to be a signed distance function.

3.4. Incorporation of the detection results

We incorporate the detection results in two ways. In its first expression, an initial contour or region has to be provided in order to initiate the evolution equation and we use these detected regions (or some processed version of them) as start regions.

In the other hand, the detection step provides also some information about the location of the aorta walls in the form of a field $p_A(x)$ of probability values of aorta walls being at position x. They can be used to bias the evolution toward the high probability values, since we expect these calcific deposit to be situated and oriented along the aorta walls. This bias, or likelihood (at that step) can be added in the numerical criterion (5) to form the following aorta wall biased criterion

$$\mathcal{H}_{AW}(\Omega) = \mathcal{H}(\Omega) + \int_\Omega f(p_A(x))\,dx \tag{10}$$

with the inpainting constraint and with f an *increasing* function: we give preference to aorta wall regions. Compared to the resulting system of equations (7,8,9) for the criterion $\mathcal{H}(\Omega)$, only the contour equation (7) is modified, in a trivial way, to accommodate for the new term in $\mathcal{H}_{AW}(\Omega)$

$$\frac{\partial \Gamma}{\partial t} = S\left(p\frac{\mathcal{H}(\Omega)}{|\Omega|} - \frac{L(I_b, I)_{|\Gamma}}{|\Omega|^p} - \lambda(I_b - I)\xi_{|\Gamma} + f \circ p_{A|\Gamma}\right)\vec{n} \tag{11}$$

the only difference in the contour evolution being the incorporation of the prior values along the contour. Here also, the detected regions are used as start regions for the evolution equation.

4. RESULTS & EXPERIMENTS

In this section we illustrate the different aspects of our approach. We present first some results on the particle filter based detection algorithm. Secondly, we illustrate the behavior of the segmentation algorithm first on a synthetic image then on some true X-rays. We then chose four fixed sets of parameters that we have used to run experiments on the two steps approach. We present results comparing the output of the detection step and the output of the two-steps process, for each set of parameters, in term of area overlap with the ground truth segmentation. Finally, we show two examples of the segmentation where the aortic walls knowledge has been incorporated (this is still an ongoing work).

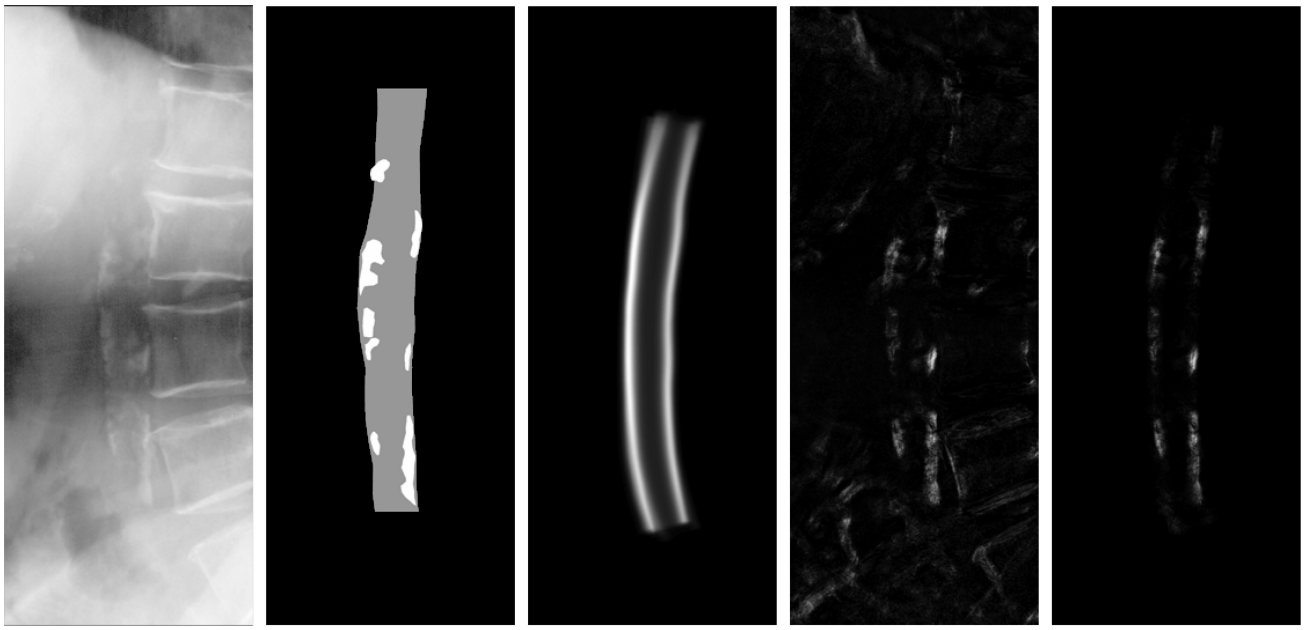

Figure 1. Example of calcification detection. a) Detail of original X-ray image b) Manual segmentation c) Spatially varying prior after ten iterations d) Original pixel classification (soft labeling) e) Shape guided pixel classification (soft labeling)

4.1. On the calcification detections

For the pixel classification, we used a feature bank of Gaussian derivatives of up to third order and at three scales (1, 4.5, and 20 pixels) with an approximate k-NN classifier.[31]

Figure 1 illustrates the detection step: it shows an X-ray of the lumbar aortic region, the ground truth calcification segmentation provided by an expert radiologist, and the differents parts of the detection mechanism: a snapshot of the shape prior after a few iterations, the original pixel classification as a map of probability values at each pixel and then the combined or shape guided classification result, also as a map of probability values, where most of the non calcification anatomical structures have been correctly eliminated.

4.2. Inpainting based segmentation

The first experiment presents the results of segmentation of an hypothetical calcification image, in a noise free situation, but with important background variation: the intensity of the plaque is 0.065, and is added to a background which intensity is modeled by a 4th order polynomial, with range [0,1]. Since no other spurious object is present in the image, an uncommitted initialization allows for a very good segmentation. This is illustrated in Figure 2. We used here a TV inpainting ($r = 1$ in energy (6)) while the area exponent in equation (5) is 0.5.

On the second example, illustrated in Figure 3, the calcification appears a bit brighter, but noise has been added. In this situation and the previous one, a run of Chan and Vese algorithm with the same initial contours and parameters a described in their original paper[12] failed.

The next experiment (Figure 4) illustrates the behavior of the active contour algorithm on a real X-ray. The segmentation is initialized with a small region which intersection with the calcification is relatively small. The contour will deform and provide finally good quality segmentation.

The last experiment of this paragraph demonstrates the transparency mechanism: we segment a calcification which bottom part blends with an anatomical structure - a hip. This is illustrated in Figure 5. We used as discrepancy measure the absolute value of pixel differences here, with a Total Variation Inpainting denoising.

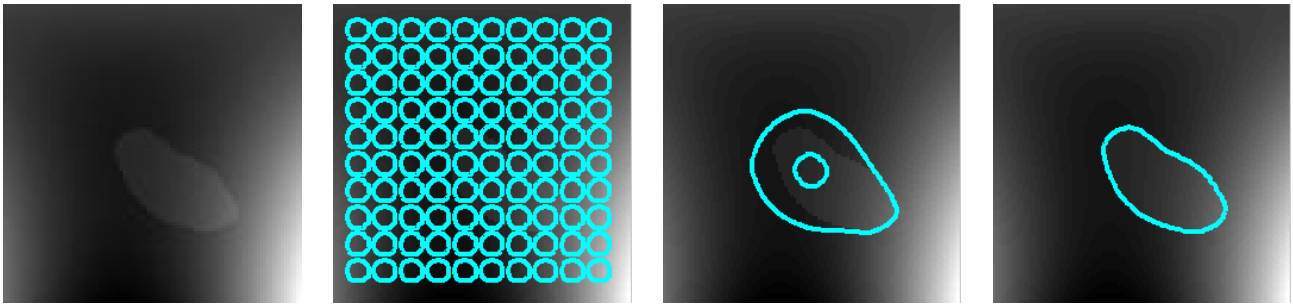

Figure 2. A noise free synthetic example. From left to right: a) the pseudo calcification, which has constant gray level value, is added on the spatially varying background, b) the original contour location guess as a collection of circles, c) the contour at the middle of evolution and d) the final contour.

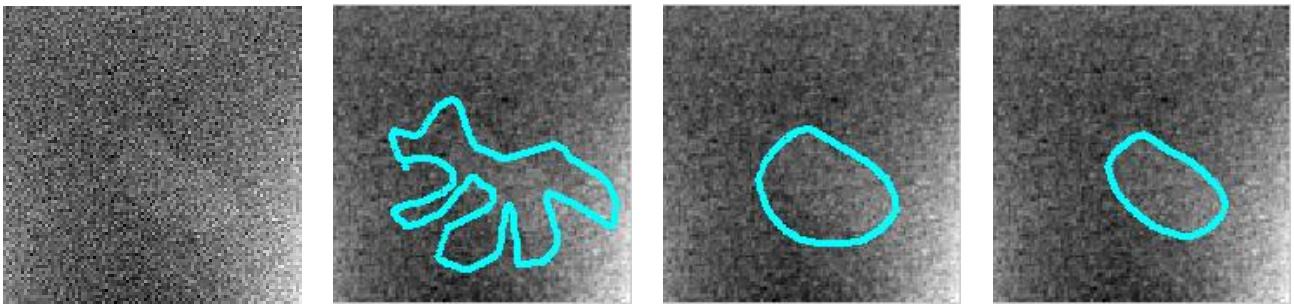

Figure 3. A noisy synthetic example. From left to right: a) the pseudo calcification, which has constant gray level value, is added on the spatially varying background with Gaussian white noise of standard deviation 15% of intensity range , b) the starting contour location, c) the contour at the middle of evolution and d) the final contour.

4.3. The simple two-steps approach.

In this paragraph we illustrate the simple two-steps approach: the segmentation is initialized from the detection step. We selected 10 X-rays and all in all 48 areas in these X-rays where the detection step provided some candidate regions. These detected regions where dilated with a flat circular structuring element of radius 2 as a preprocessing step. We ran the segmentation algorithm with 4 sets of parameters (p, r, λ) where p is the area penalization weight in formula (5), r is the regularization norm type in the inpainting energy (6) and λ is the data attachment term in the same inpainting energy. We ran 200 iterations of the algorithm and computed the average area overlap (AAO) at iteration 50, 100, 150 and 200 – the area overlap measure we use for a candidate region R with respect to the ground truth G is given by

$$\mathrm{AO}(R, G) = \frac{|R \cap G|}{|R \cup G|}.$$

The parameter values and results are summarized in table 1. The best results are provided by the last set of parameters, for 100 iterations. For comparison we computed the AAO when respectively dilating and closing the detected areas, with flat circular structural elements with radius ranging from 1 to 40. The best AAO was 0.3866 and was obtained using a morphological closing of the detected regions with a disk of radius 13. The best AAO with our segmentation method is 0.4214.

The next figure (Figure 6) shows some of the selected areas, corresponding ground truth, detected areas and segmentation results.

4.4. Some aorta wall biased segmentation

We are currently working on the segmentation biased by the aortic wall data. Our results are still preliminary and we provide two illustrations in the following figure 7 where we run the segmentation starting from the

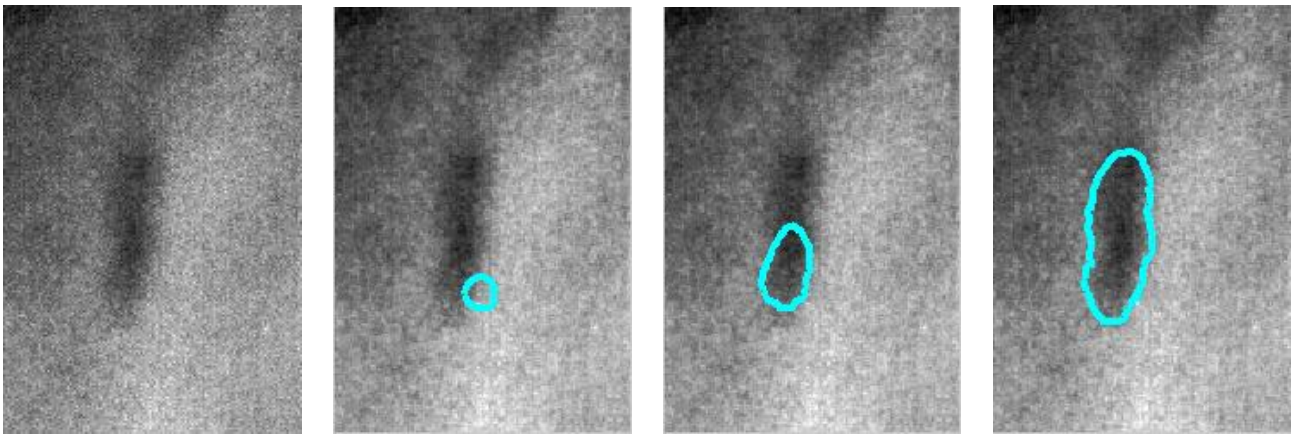

Figure 4. Evolution of the active contour in a real X-ray. a) a subimage of the original X-ray (inverted), b) the starting contour, with only small overlap with the calcific deposit. c) The contour has "entered" the calcific deposit and start growing, d) the final segmentation.

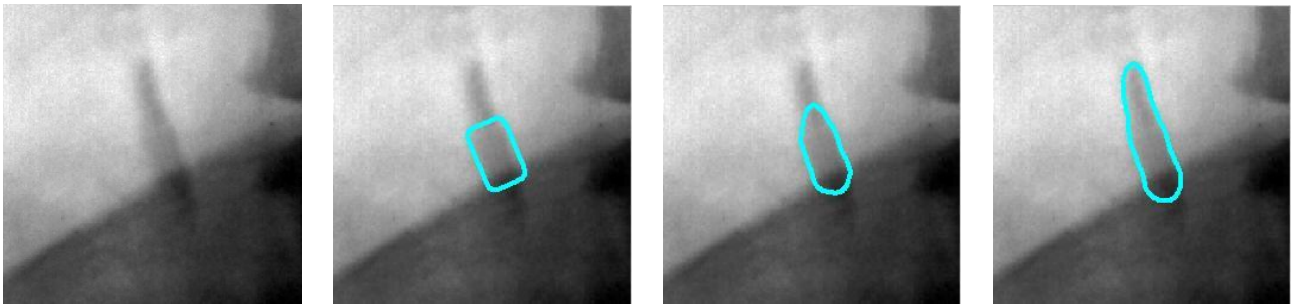

Figure 5. Evolution of the active contour in a real X-ray: the use of TV inpainting in the background substraction allows for reconstruction of the hip with in turns provides a a) a subimage of the original X-ray (inverted), b) the starting contour, with only small overlap with the calcific deposit. c) The contour has "entered" the calcific deposit and start growing, d) the final segmentation.

detected calcified area both with and without bias toward the aortic wall. While the results of the top row seem satisfactory, the second row shows an artifact of the bias which has "moved" the calcification boundaries toward the vertical direction, although the result is clearly better than the one obtained without the bias toward the aortic wall.

5. CONCLUSION

In this work we describe a detection/segmentation algorithm aiming at segmenting and quantifying the degree of atherosclerosis. It represents an important step towards the construction of a fully automated system for segmenting and measuring the extent of calcification in the lumbar aortic region from radiographs. This combines different techniques, pixel classification and active shape models within a particle filtering framework, and active region / inpainting based segmentation within a level set framework. The use of somewhat sophisticated techniques is necessary due to the the nature of 2D X-ray imaging and calcific deposits, making the task a complex one, but preliminary results are very encouraging and we are working on larger scale experimentation and medical evaluation. We are also working on incorporation of aortic wall data in the segmentation, using the simple form that was described in this paper, as well as a more sophisticated in term of geometric content.

6. ACKNOWLEDGMENTS

We would like to thank L. B. Tankó and C. Christiansen of the Center for Clinical and Basic Research (CCBR A/S), Denmark, for providing the data set and manual segmentation used in this paper, L. A. Conrad-Hansen

	p	r	λ	AAO 50	AAO 100	AAO 150	AAO 200
Parameter set 1	0.5	1	0.1	0.3992	0.3786	0.3574	0.3384
Parameter set 2	0.75	1	0.1	0.4012	0.3848	0.3714	0.3611
Parameter set 3	0.5	2	0.01	0.4169	0.4145	0.4083	0.4017
Parameter set 4	0.75	2	0.01	0.4193	**0.4214**	0.4181	0.4138

Table 1. The different parameters sets used in our batch experiments and the Average Area Overlap results for 50, 100, 150 and 200 iterations.

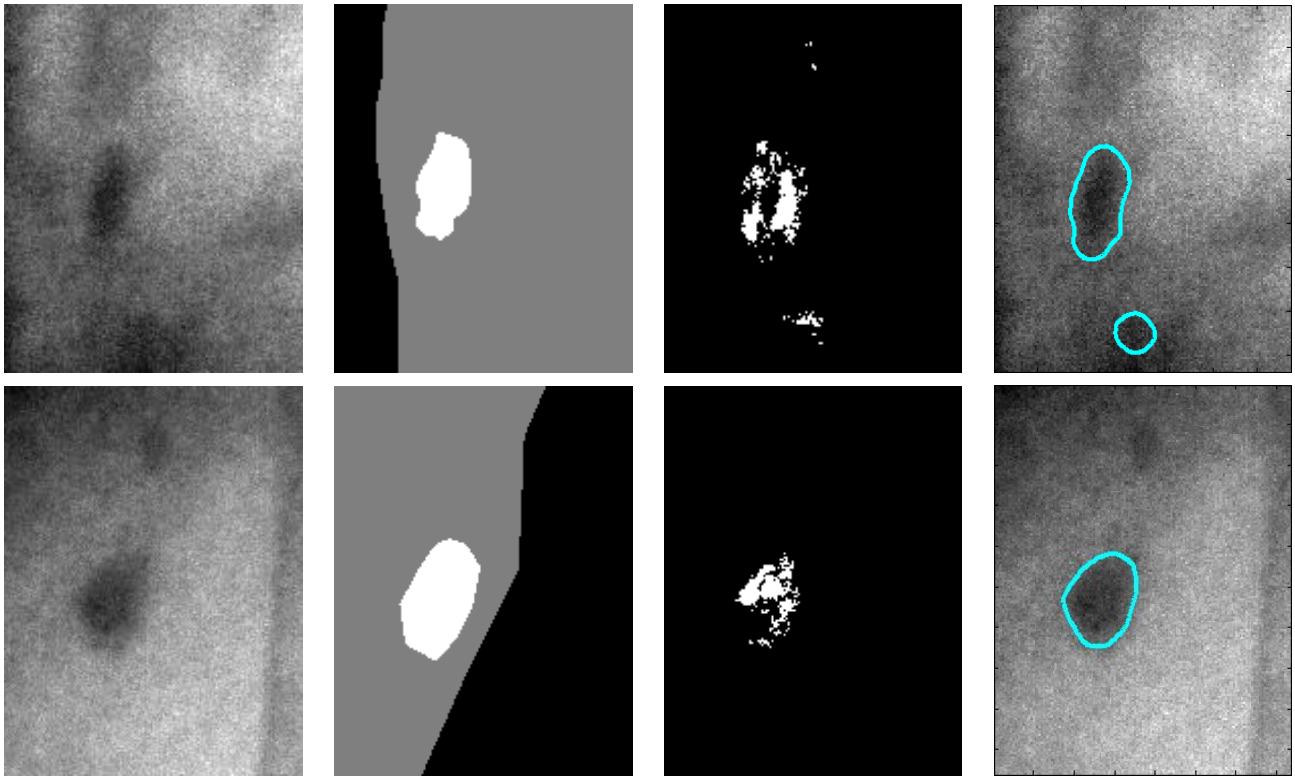

Figure 6. Two examples of the 2-step process. First column: original views. Second column: ground truth segmentations. Third column: detection. Last column: segmentation.

and M. T. Lund for providing the software to perform manual segmentation and CCBR A/S Denmark for funding. Part of this work was performed while the authors were with the Image Group of the IT University of Copenhagen, within the CATIA project, funded by CCBR A/S and Nordic Bioscience Diagnostics A/S.

REFERENCES

1. D. Eggen, J. Strong, and H. McGill, "Calcification in the abdominal aorta: relationship to race, sex, and coronary atherosclerosis," *Arch Pathol* **78**, pp. 575–583, 1964.
2. J. Wolffe and E. Siegal, "X-ray of the abdominal aorta in detection of atherosclerosis," *Clin Med* **69**, pp. 401–406, 1962.
3. P. Wilson and et al., "Abdominal aortic calcific deposits are an important predictor of vascular morbidity and mortality," *Circulation* **103**, pp. 1529–1534, 2001.
4. J. Witteman, V. V. S. J.L.C, and H. Valkenburg, "Aortic calcification as a predictor of cardiovascular mortality," *Lancet* **2**, pp. 1120–2, 1986.
5. J. C. M. Witteman and et al., "Aortic calcified plaques and cardiovascular disease (the framingham study)," *Am. J. Cardiol* **6**, pp. 1060–4, 1990.

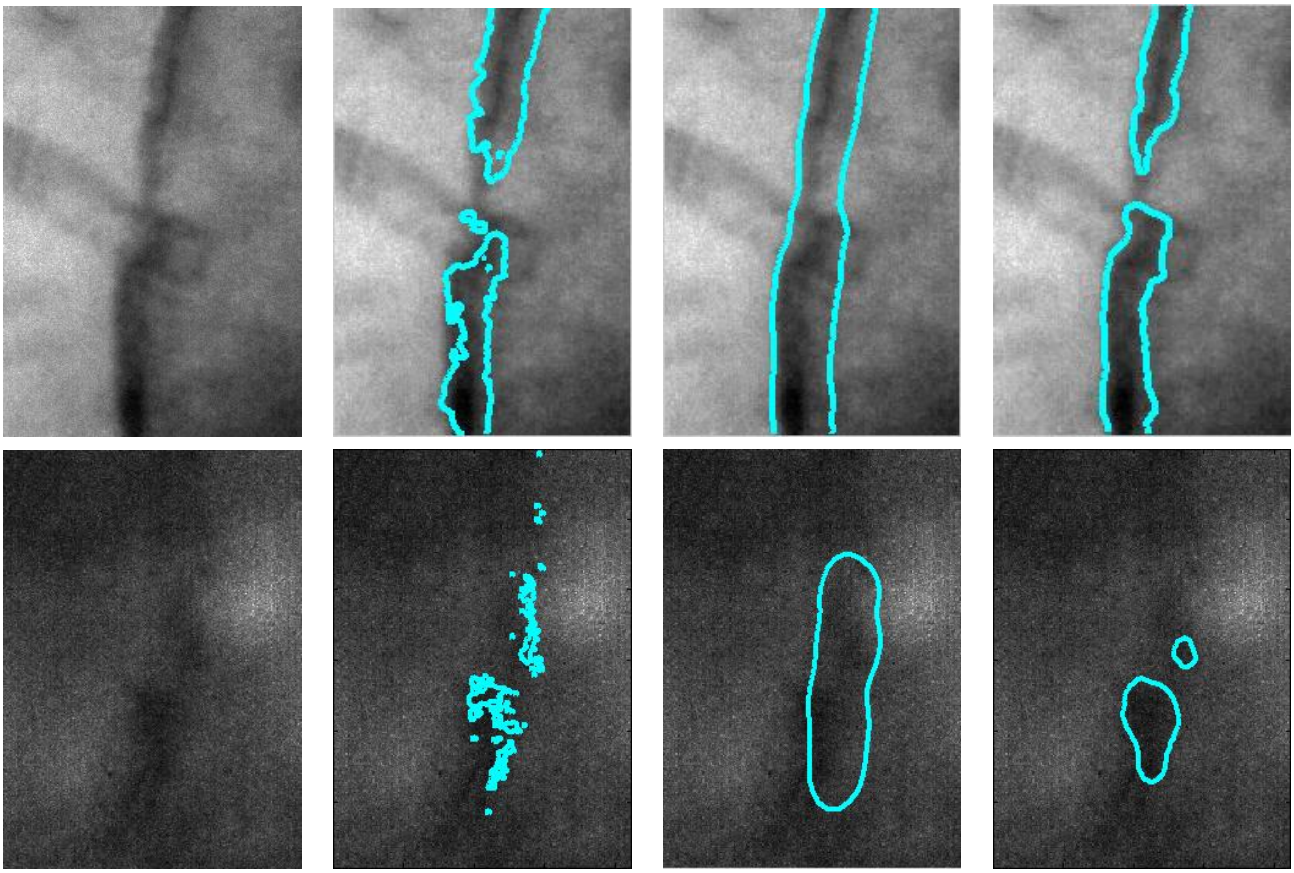

Figure 7. Segmentation with and without aorta knowledge: First column: original images. Second column: detected areas. Third column: segmentation with bias toward aortic walls. Last column: segmentations without the aortic wall bias

6. L. B. Tanko and et al., "Peripheral adiposity exhibits an independant dominant antiatherogenic effect in elderly women," *Circulation* **107**, pp. 1626–1632, 2003.
7. D. Kiel and et al., "Bone loss and the progression of abdominal aortic calcification over a 25 year period: The framingham heart study," *Calcified Tissue International* **68**, pp. 271–276, 2001.
8. M. Higgins, Marvel, "Quantification of calcification in atherosclerotic lesions," *Arterioscler. Thromb. Vasc. Biol.* **25**, pp. 1567–1576, 2005.
9. L. Kauppila and et al., "New indices to classify location, severity and progression of calcific lesions in the abdominal aorta: a 25-year follow-up study," *Atherosclerosis* **132**, pp. 245–250, 1997.
10. M. de Bruijne and M. Nielsen, "Image segmentation by shape particle filtering," in *International Conference on Pattern Recognition*, 2004.
11. M. de Bruijne, "Shape Particle Guided Tissue Classification," in *Mathematical Methods in Biomedical Image Analysis (MMBIA)*, P. Golland and D. Rueckert, eds., 2006.
12. T. Chan and L. Vese, "Active contours without edges," *IEEE Transactions on Image Processing* **10**, pp. 266–277, Feb. 2001.
13. F. Lauze and M. Nielsen, "From Inpainting to Active Contours," in *Proceedings of the third IEEE workshop on Variational, Geometric and Level Set Methods in Computer Vision*, N. P. et al., ed., pp. 97–108, Springer, (Bejing, China), Oct. 2005. LNCS 3752.
14. L. Conrad-Hansen, M. de Bruijne, F. Lauze, M. Nielsen, and L. Tánkó, "Quantizing calcification in the lumbar aorta on 2-d lateral x-ray images using tv inpainting," in *Computer Vision for Biomedical Image Applications*, C. Z. Yanxi Liu, Tianzi Jiang, ed., **3765**, pp. 409–418, Springer-Verlag, 2005.

15. L. Conrad-Hansen, M. de Bruijne, F. Lauze, M. Nielsen, and L. Tánkó, "A pixelwise inpainting based refinement scheme for quantizing calcification in the lumbar aorta on 2d lateral x-ray images," in *miip*, J. Reinhardt and J. Pluim, eds., *Proceedings of the SPIE Medical Imaging Conference* **6144**, SPIE Press, 2006. In press.
16. R. O. Duda, P. E. Hart, and D. G. Stork, *Pattern Classification, Second Edition*, John Wiley and Sons, 2001.
17. M. de Bruijne and M. Nielsen, "Shape Particle Filtering for Image Segmentation," in *Proceedings of the 7th Medical Image Computing & Computer-Assisted Intervention Conference*, D. H. C. Barillot and P. Hellier, eds., pp. 186–175, (Saint-Malo, France), 2004. LNCS 3216.
18. T. C. M. Roberts and J. Adams, "Automatic Segmentation of Lumbar Vertebrae on Digitised Radiographs Using Linked Active Appearance Models," **1**, pp. 120–124, 2006.
19. M. Kass, A. Witkin, and D. Terzopoulos, "Snakes: Active contour models," in *First International Conference on Computer Vision*, pp. 259–268, (London), June 1987.
20. L. D. Cohen and I. Cohen, "Finite-Element Methods for Active Contour Models and Balloons for 2-D and 3-D Images.," *IEEE Transactions on Pattern Analysis and Machine Intelligence* **15**(11), pp. 1131–1147, 1993.
21. C. Xu and J. L. Prince, "Gradient Vector Flow: A New External Force for Snakes.," in *International Conference on Computer Vision and Pattern Recognition*, pp. 66–, 1997.
22. V. Caselles, R. Kimmel, and G. Sapiro, "Geodesic active contours," in *Proceedings of the5th International Conference on Computer Vision*,[32] pp. 694–699.
23. S. Kichenassamy, A. Kumar, P. Olver, A. Tannenbaum, and A. Yezzi, "Gradient flows and geometric active contour models," in *Proceedings of the5th International Conference on Computer Vision*,[32] pp. 810–815.
24. D. Mumford and J. Shah, "Optimal approximations by piecewise smooth functions and associated variational problems," *Communications on Pure and Applied Mathematics* **42**, pp. 577–684, 1989.
25. G. Aubert, M. Barlaud, S. Jehan-Besson, and O. Faugeras, "Image segmentation using active contours: Calculus of variations or shape gradients?," *SIAM Journal of Applied Mathematics* **63**(6), pp. 2128–2154, 2003.
26. N. Paragios and R. Deriche, "Geodesic active regions: a new paradigm to deal with frame partition problems in computer vision," *Journal of Visual Communication and Image Representation, Special Issue on Partial Differential Equations in Image Processing, Computer Vision and Computer Graphics* **13**, pp. 249–268, march/june 2002.
27. A. V. Oppenheim, "Superpostion in a Class of Nonlinear Systems," in *Proceedings of IEEE International Convention*, pp. 171–177, (New York, USA), 1964.
28. T. Chan and J. Shen, "Mathematical models for local nontexture inpainting," *SIAM journal of appl. Math* **62**(3), pp. 1019–1043, 2002.
29. M. Delfour and J.-P. Zolésio, *Shapes and Geometries*, Advances in Design and Control, Siam, 2001.
30. J. Sethian, *Level Set Methods and Fast Marching Methods: Evolving Interfaces in Computational Geometry, Fluid Mechanics, Computer Vision, and Materials Sciences*, Cambridge Monograph on Applied and Computational Mathematics, Cambridge University Press, 1999.
31. S. Arya, D. Mount, n. Netanyahu, R. Silverman, and A. Wu, "An Optimal Algorithm for Approximate Nearest Neighbor Searching," *Journal of the ACM* **45**, pp. 891–923, 1998.
32. *ICCV 95*, (Boston, MA), IEEE Computer Society Press, June 1995.